

# Piecewise Interaction Picture Density Matrix Quantum Monte Carlo

William Van Benschoten<sup>1</sup> and James J. Shepherd<sup>1, a)</sup>

*Department of Chemistry, University of Iowa*

(Dated: 11 April 2022)

The density matrix quantum Monte Carlo (DMQMC) set of methods stochastically samples the exact  $N$ -body density matrix for interacting electrons at finite temperature. We introduce a simple modification to the interaction picture DMQMC method (IP-DMQMC) which overcomes the limitation of only sampling one inverse temperature point at a time, instead allowing for the sampling of a temperature range within a single calculation thereby reducing the computational cost. At the target inverse temperature, instead of ending the simulation, we incorporate a change of picture away from the interaction picture. The resulting equations of motion have piecewise functions and use the interaction picture in the first phase of a simulation, followed by the application of the Bloch equation once the target inverse temperature is reached. We find that the performance of this method is similar to or better than the DMQMC and IP-DMQMC algorithms in a variety of molecular test systems.

## I. INTRODUCTION

Electrons interacting in the presence of a finite temperature play an important role in many applications including the study of planetary cores<sup>1,2</sup>, plasma physics<sup>3,4</sup>, laser experiments<sup>5</sup>, and condensed phases of matter<sup>6,7</sup>. There has been a recent push to take methods which are effective for solving ground state electronic structure problems, especially quantum chemical wavefunction methods, and adapting them to treat finite temperature. Examples of this include perturbation theories<sup>8–12</sup> and coupled cluster techniques<sup>13–21</sup>. Other *ab initio* methods under active development include ft-DFT<sup>22–26</sup> and various flavors of Green’s function methods<sup>27–33</sup> such as self-consistent second-order perturbation theory (GF2) and *GW* theory.

Additionally, embedding theories, which break the calculation up into an exactly treated subsystem and an approximately treated bath, have been proposed.<sup>34–46</sup> There are also a variety of quantum Monte Carlo methods which work with finite temperature ensembles of electrons, such as path integral Monte Carlo<sup>47–54</sup>, determinant quantum Monte Carlo (DQMC)<sup>55,56</sup>, finite temperature auxiliary field quantum Monte Carlo (ft-AFQMC)<sup>57–61</sup>, and Krylov-projected quantum Monte Carlo<sup>62</sup>.

The method we use here, density matrix quantum Monte Carlo (DMQMC), stochastically samples the exact  $N$ -body density matrix in a finite basis.<sup>63</sup> It is the finite temperature equivalent to FCIQMC<sup>64</sup>, which has been very successful in treating ground-state problems to FCI accuracy. In the original paper,<sup>63</sup> DMQMC calculated thermal quantities for the Heisenberg model including the energy and Renyi-2 entropy. Thereafter, interaction picture DMQMC (IP-DMQMC) was introduced which introduced a change of picture allowing for the diagonal (and trace) of the density matrix to be sampled much more accurately than DMQMC.<sup>65</sup> It does so

by simulating one temperature at a time and starting at an approximate density matrix for that temperature. After being developed to use the initiator approach,<sup>65</sup> which was also adapted from the ground-state FCIQMC version<sup>66</sup>, IP-DMQMC benchmarked the warm dense electron gas alongside path integral Monte Carlo approaches to obtain a finite-temperature local density approximation functional.<sup>67–69</sup> In addition to these successes, IP-DMQMC showed promise in initial applications to molecular systems<sup>70</sup> and its sign problem showed to be similar to that of FCIQMC.<sup>71</sup> Recently DMQMC has also inspired a new method, fixed point quantum Monte Carlo, which samples the ground state density matrix.<sup>72</sup>

In this work we seek to extend IP-DMQMC by continuing the simulation after the target inverse temperature is reached. We find that continuing to apply the Bloch equation as the propagator allows for the rest of the temperature-dependent energy to be found. This is possible because IP-DMQMC reaches the exact density matrix (on average) once it reaches a target temperature. This paper starts with an introduction to DMQMC methods followed by a derivation of the new piecewise IP-DMQMC propagation equations (which we call PIP-DMQMC). Next we test PIP-DMQMC for a set of molecular systems making comparison with DMQMC, IP-DMQMC, and finite temperature full configuration interaction (ft-FCI).<sup>73</sup> We then explore how PIP-DMQMC can be combined with the initiator approximation (i-PIP-DMQMC) and that these can be used to treat larger systems that cannot be exactly diagonalized. We close by noting how the compute time cost of simulating a range of evenly-spaced target inverse temperatures in IP-DMQMC scales roughly as the square of the largest target inverse temperature sampled, while PIP-DMQMC samples the same range with linear scaling.

<sup>a)</sup>Electronic mail: [james-shepherd@uiowa.edu](mailto:james-shepherd@uiowa.edu)

## II. METHODS

In this section, we begin with a review of the DMQMC algorithm including key algorithmic definitions and the initiator approximation. We then describe how IP-DMQMC differs from DMQMC and the sum-over-states methods we used here (ft-FCI and THF). Section III introduces our new method PIP-DMQMC.

### A. DMQMC

The DMQMC set of methods<sup>63</sup> was a generalization of full configuration interaction quantum Monte Carlo (FCIQMC)<sup>64</sup> to solving the  $N$ -body density matrix at finite temperature:

$$\hat{\rho}(\beta) = e^{-\beta\hat{H}}, \quad (1)$$

where  $\beta = 1/kT$ . The density matrix is written in a finite basis in imaginary time:

$$\hat{\rho}(\beta) \rightarrow \hat{f}(\tau) = \sum_{ij} f_{ij}(\tau) |D_i\rangle\langle D_j|, \quad (2)$$

where  $D_i$  are the orthogonal Slater determinants. These determinants are formed from the orbitals calculated during a ground state Hartree–Fock (HF) calculation. In DMQMC, the density matrix is represented by walkers which are said to be on sites in the simulation. One site, labelled with an  $i$  and  $j$  index, represents each  $|D_i\rangle\langle D_j|$  and the number of walkers at site  $ij$  is proportionate to  $f_{ij}$ . The goal is to find

$$E(\beta) = \frac{\text{Tr}[\hat{H}\hat{\rho}(\beta)]}{\text{Tr}[\hat{\rho}(\beta)]}, \quad (3)$$

by taking an average over  $N_\beta$  separate simulations (these are termed  $\beta$  loops).

In DMQMC, the simulation is started from a random distribution of walkers along the diagonal of the density matrix, which represents the exact density matrix at high temperature:

$$\hat{f}(\tau = 0) = \mathcal{K}. \quad (4)$$

The symmetrized Bloch equation is then applied in the form

$$\frac{d\hat{f}(\tau)}{d\tau} = -\frac{1}{2} \left[ \hat{H}\hat{f}(\tau) + \hat{f}(\tau)\hat{H} \right], \quad (5)$$

and using the Bloch equation with a finite  $\Delta\tau$  yields the equations of motion:

$$f_{ij}(\tau + \Delta\tau) = f_{ij}(\tau) \left[ 1 + \Delta\tau S \right] - \frac{\Delta\tau}{2} \sum_k [H_{ik}f_{kj}(\tau) + f_{ik}(\tau)H_{kj}], \quad (6)$$

where a constant shift ( $S$ ) is applied to each matrix element, and is dynamically updated during the simulation to control the walker population. At every time step for DMQMC,  $f_{ij}(\tau)$  is equivalent to sampling  $\rho_{ij}(\beta)$  at  $\beta = \tau$ .

Equation 6 is interpreted in the DMQMC algorithm by steps referred to as spawning, cloning/death, and annihilation. This is key for the computational efficiency of the method and are described in more detail in the supplementary information. Spawning stochastically samples the  $\sum_k$  taking advantage of the sparsity of  $\hat{H}$  and the death/cloning steps control the walker population/memory cost.

The shift is updated at intervals using:

$$S(\tau + \Delta\tau) = S(\tau) - \frac{\zeta}{A\Delta\tau} \ln \left( \frac{N_w(\tau + \Delta\tau)}{N_w(\tau)} \right). \quad (7)$$

In this equation  $A$  is the number of imaginary time steps (iterations of Eq. (6)) between updates,  $N_w$  is the walker population, and  $\zeta$  is a damping parameter. For this study we used  $A = 10$  and  $\zeta = 0.05$ .

The initiator approximation<sup>66</sup> was developed in FCIQMC and subsequently adapted for DMQMC.<sup>74</sup> The initiator approximation is a way to stabilize the sign problem, (which arises in numerical methods due to coefficients in the solution having both positive and negative values). In DMQMC, two parameters are introduced: a spawned walker threshold,  $n_{\text{add}}$ , and a excitation number cutoff,  $n_{\text{ex}}$ . The population of sites occupied in the simulation (the  $ij$  indices) is divided into initiators which have a population that is  $\geq n_{\text{add}}$  or an excitation number  $\leq n_{\text{ex}}$ . To find the excitation number for the  $ij$  site, the excitations between  $D_i$  and  $D_j$  in  $|D_i\rangle\langle D_j|$  are used (i.e. if  $D_i$  was a double excitation of  $D_j$ , this would count as  $n_{\text{ex}} = 2$ ). Spawning events to sites without walkers are then allowed only if they come from initiator sites or two spawning events with the same sign arrive at once to a single site. This introduces a population-and-system-dependent systematic error to the simulation that is removed in the limit of an infinite total walker population ( $N_w \rightarrow \infty$ ). This is typically referred to as being systematically improvable.<sup>66,74–79</sup> We used  $n_{\text{add}} = 3.0$  and  $n_{\text{ex}} = 2$  in this study, which came from preliminary investigations and was consistent with previously used values for the uniform electron gas.<sup>74</sup>

### B. IP-DMQMC

In IP-DMQMC the simulation starts with a known density matrix:

$$\hat{f}(\tau = 0) = e^{-\beta\tau\hat{H}^{(0)}}, \quad (8)$$

where  $\hat{H}^{(0)}$  is the diagonal of  $\hat{H}$ . Then, the simulation proceeds in imaginary time aiming to sample the exact density matrix at a certain  $\beta$  (the target  $\beta$  or  $\beta_T$ ). Over

the simulation IP-DMQMC samples

$$\hat{f}(\tau) = e^{-(\beta_T - \tau)\hat{H}^{(0)}} e^{-\tau\hat{H}} \quad (9)$$

instead of sampling  $e^{-\tau\hat{H}}$ . Each IP-DMQMC calculation requires a  $\beta_T$  to be specified which is the inverse temperature at which we wish to calculate the density matrix.

The initial density matrix  $e^{-\beta\hat{H}^{(0)}}$  is stochastically sampled. The protocol is as follows. First, select a determinant by occupying  $N$  orbitals at random, and then accepting this selection according to the product of its normalized Fermi-Dirac weights:

$$P = \prod_{p \in \text{occ}} n_p \prod_{p \in \text{unocc}} 1 - n_p, \quad (10)$$

where  $p$  refers to an orbital index. The abbreviations occ and unocc respectively refer to occupied and unoccupied orbital indices. The normalized Fermi-Dirac weights are calculated as:

$$n_i = \frac{1}{e^{\beta(\epsilon_i - \mu)} + 1}, \quad (11)$$

where  $\epsilon_i$  are the single-particle energies (ground-state HF orbital eigenvalues), and  $\mu$  is a temperature-dependent chemical potential calculated so that the weights sum to the particle number<sup>65</sup>. Accepting only those orbital configurations which conserve the particle number and symmetry ensures a canonical distribution is obtained.

The Fermi-Dirac weights sample  $e^{-\beta\hat{H}'}$ , where  $\hat{H}'$  is diagonal in the Slater Determinant basis and is made from non-interacting orbitals that have as their orbital energies the HF one-particle eigenvalues. Noting that  $e^{-\beta\hat{H}'} \neq e^{-\beta\hat{H}^{(0)}}$ , the walker population on that site is then set to the difference between the  $e^{-\beta\hat{H}^{(0)}}$  and the  $e^{-\beta\hat{H}'}$ , normalized such that selection of  $H_{00}^{(0)}$  is given a weight of 1, then the population is stochastically rounded to a predefined cutoff (0.01 in this work).<sup>80</sup> Annihilation is performed on the spawned walkers, prior to propagation, once the desired walker population is reached from initialization.

The propagator in IP-DMQMC is

$$\frac{d\hat{f}(\tau)}{d\tau} = \hat{H}^{(0)}\hat{f}(\tau) - \hat{f}(\tau)\hat{H}, \quad (12)$$

and because the matrix Eq. (9) contains  $\hat{H}^{(0)}$ ,  $\hat{H}^{(0)}$  appears in our propagator. The absence of a  $\frac{1}{2}$  when compared to DMQMC (Eq. (5)) is because the propagator is asymmetric to save the computational cost of storing additional factors<sup>81</sup>. Using the propagator with a finite  $\Delta\tau$ , and including a constant shift ( $S$ ) for controlling the population the equations of motion is written as:

$$f_{ij}(\tau + \Delta\tau) = f_{ij}(\tau) [1 + \Delta\tau S] - \Delta\tau \sum_k \left[ -H_{ik}^{(0)} f_{kj}(\tau) + f_{ik}(\tau) H_{kj} \right]. \quad (13)$$

In IP-DMQMC,  $f_{ij}(\tau)$  is equivalent to sampling  $\rho_{ij}(\beta)$  only at  $\tau = \beta_T$ .

### C. ft-FCI and THF

In this work, it is useful to have exact finite temperature electronic energies to benchmark the QMC methods. Therefore, we use a sum-over-states method to generate the exact energy (within a basis), known as ft-FCI.<sup>73</sup> The finite temperature energy is

$$E = \frac{\sum_i E_i e^{-\beta E_i}}{\sum_i e^{-\beta E_i}}, \quad (14)$$

where  $E_i$  are the energy eigenstates resulting from the exact diagonalization (FCI) of  $\hat{H}$ .

In addition to ft-FCI, we calculate an energy referred to as thermal HF (THF), which is a sum over Boltzmann weighted Slater determinants:

$$E^{(0)} = \frac{\sum_i E_i^{(0)} e^{-\beta E_i^{(0)}}}{\sum_i e^{-\beta E_i^{(0)}}}, \quad (15)$$

$E_i^{(0)}$  is the energy of a single Slater determinant comprised of the canonical orbitals from a ground-state HF calculation. In our case, this means  $E_i^{(0)} = H_{ii}$ , or the diagonal of the FCI Hamiltonian prior to diagonalization. To calculate the thermal correlation energy, we subtract THF from ft-FCI. When the correlation energy is negative, ft-FCI is lower in energy than THF.

### III. PIP-DMQMC

The benefit of IP-DMQMC is that the starting density matrix is much closer to the density matrix at  $\beta_T$  and the change of the density matrix over the simulation is reduced. However, the limitation of this approach is that a single target temperature must be simulated at a time and, consequently, this means that more computer time is spent in the calculation trying to reach  $\beta_T$  than collecting statistics at  $\beta_T$ . Our method here is designed to overcome this limitation.

Noting that the density matrix in an IP-DMQMC simulation is exact at  $\tau = \beta_T$ , *i.e.*

$$f_{ij}(\tau = \beta_T) = \rho_{ij}(\beta_T), \quad (16)$$

application of the Bloch equation on this IP-DMQMC density matrix would allow us to determine  $\hat{\rho}(\beta_T + \Delta\tau)$ . Repeated application of the Bloch equation will generally allow the density matrix at  $\beta > \beta_T$  to be found.

In piecewise IP-DMQMC (PIP-DMQMC) we therefore start with the same density matrix as in IP-DMQMC,

$$\hat{f}(\tau = 0) = e^{-\beta_T \hat{H}^{(0)}}, \quad (17)$$

and the propagator can be expressed as,

$$\frac{d\hat{f}(\tau)}{d\tau} = \Theta(\beta_T - \tau) \left[ \hat{H}^{(0)} f(\tau) - \hat{f}(\tau) \hat{H} \right] - \frac{1}{2} [1 - \Theta(\beta_T - \tau)] \left[ \hat{H} \hat{f}(\tau) + \hat{f}(\tau) \hat{H} \right], \quad (18)$$

where  $\Theta(x)$  is a Heaviside step function defined as being equal to 1 for  $x > 0$  and 0 otherwise. We note that the propagator is always asymmetric in the IP-DMQMC part of the simulation as symmetrizing IP-DMQMC is non-trivial.<sup>81</sup> In the Bloch equation above, the propagator is

explicitly symmetrized, which is where the factor of  $\frac{1}{2}$  comes from.

A formulation where the Bloch equation is asymmetric is also possible:

$$\frac{d\hat{f}(\tau)}{d\tau} = \Theta(\beta_T - \tau) \left[ \hat{H}^{(0)} f(\tau) - \hat{f}(\tau) \hat{H} \right] - [1 - \Theta(\beta_T - \tau)] \hat{f}(\tau) \hat{H}. \quad (19)$$

Using these propagators with a finite  $\Delta\tau$ , the equations of motion are:

$$f_{ij}(\tau + \Delta\tau) = \begin{cases} f_{ij}(\tau)[1 + \Delta\tau S] - \Delta\tau \sum_k \left[ -H_{ik}^{(0)} f_{kj}(\tau) + f_{ik}(\tau) H_{kj} \right] & \tau < \beta_T; \\ f_{ij}(\tau)[1 + \Delta\tau S] - \frac{\Delta\tau}{2} \sum_k \left[ H_{ik} f_{kj}(\tau) + f_{ik}(\tau) H_{kj} \right] & \tau \geq \beta_T \end{cases} \quad (20)$$

$$f_{ij}(\tau + \Delta\tau) = \begin{cases} f_{ij}(\tau)[1 + \Delta\tau S] - \Delta\tau \sum_k \left[ -H_{ik}^{(0)} f_{kj}(\tau) + f_{ik}(\tau) H_{kj} \right] & \tau < \beta_T; \\ f_{ij}(\tau)[1 + \Delta\tau S] - \Delta\tau \sum_k f_{ik}(\tau) H_{kj} & \tau \geq \beta_T \end{cases}. \quad (21)$$

In Eq. (20), the IP-DMQMC equations of motion (Eq. (13)) is used for the sub-domain before the target beta is reached ( $\tau < \beta_T$ ) and the symmetric Bloch equation (Eq. (6)) is used subsequently ( $\tau \geq \beta_T$ ). In Eq. (21), the formalism drops the symmetrization in the Bloch equation.

Which of these equations of motion, symmetric or asymmetric, gets used tends to be based on preliminary calculations and prior knowledge. As in the original DMQMC algorithm, symmetric propagation should generally result in less stochastic noise but may also raise the plateau.<sup>71</sup> This is consistent with what we found in preliminary calculations: the asymmetric propagation is effective without the initiator approximation and symmetric propagation is effective with the initiator approximation.

In PIP-DMQMC,  $f_{ij}(\tau)$  is equivalent to sampling  $\rho_{ij}(\beta)$  at  $\tau \geq \beta_T$ . The key result here is that piecewise propagation has the potential benefits of IP-DMQMC – skipping initialization on the identity matrix – while also allowing for continued propagation using the Bloch equation to higher values of  $\beta$ . Below, we mainly test PIP-DMQMC simulations using  $\beta_T = 1.0$ , but we also examine the effects of changing  $\beta_T$ . Finally, we also note in passing that when the total  $\beta$  simulated in PIP-DMQMC is  $\beta_T$ , the simulation reverts back to IP-DMQMC, thus we would expect these to be equivalent when the random number seed is fixed.

#### IV. CALCULATION DETAILS

The PIP-DMQMC algorithm was implemented in the HANDE-QMC<sup>82</sup> package. The molecular systems used were: Be/aug-cc-pVDZ, BeH<sub>2</sub> Be/cc-pVDZ H/DZ, equilibrium H<sub>8</sub>/STO-3G, equilibrium H<sub>4</sub>/cc-pVDZ, stretched H<sub>8</sub>/STO-3G, N<sub>2</sub>/STO-3G, LiF/STO-3G, CO/STO-3G, HCN/STO-3G, HBCH<sub>2</sub>/STO-3G, H<sub>2</sub>O/cc-pVDZ and CH<sub>4</sub>/cc-pVDZ. Geometries are provided in the supplementary information and come from a variety of sources.<sup>64,71,83–88</sup> Molecular integral files for the one- and two-particle interactions organized by orbital indices are generated with Molpro.<sup>89</sup> HANDE-QMC was used to run DMQMC, IP-DMQMC and PIP-DMQMC and to generate the FCI and  $\hat{H}^{(0)}$  eigenspectrum for ft-FCI and THF respectively. A python script was used to perform the sum-over-states method for ft-FCI and THF. Other simulation parameters are included in our data repository and supporting information.

#### V. RESULTS AND DISCUSSION

In order to validate PIP-DMQMC, we set a target accuracy for the energy of a 1 millihartree difference to the ft-FCI energy, which is the standard for high accuracy approaches in QMC for the ground state. We note in passing that this may be too high of an accuracy for finite temperature applications. We measured the accuracy for a range of test systems which we could treat with exact diagonalization. The number of density matrix elements (the square of the determinants in the space) for these systems range from  $10^5$  to  $10^8$ . As well

as PIP-DMQMC, four other calculations were performed: DMQMC, IP-DMQMC, ft-FCI, and THF. For THF, the orbitals and eigenvalues are frozen in the ground state. This is opposed to the traditional thermal Hartree–Fock method where the orbitals and eigenvalues are self consistently calculated at the given temperature. For this reason, THF is a thermal Hartree–Fock like mean-field method.<sup>74</sup>

In each of the DMQMC-type calculations, the walker population was set above the DMQMC plateau,<sup>71</sup> which is a system-specific number of walkers required to overcome the sign problem, and the initiator adaptation was not used. The walker numbers used ranged from  $5 \times 10^5$  to  $10^7$  depending on the plateau estimated for each system by running a single calculation with no shift ( $S = 0$  in Eq. (6) throughout the simulation). Energies are reported as averages over 100  $\beta$ -loops ( $N_\beta = 100$ ).

Preliminary investigations showed that systematic errors were slightly smaller in magnitude for asymmetric propagation (Eq. (21)) in PIP-DMQMC (with no initiator approximation) compared to symmetric propagation (Eq. (20)). This is consistent with the asymmetric DMQMC propagators having a smaller plateau, and for this reason we used asymmetric propagation (Eq. (21)) in these tests.<sup>71</sup>

A representative example of our set, the  $\text{BeH}_2$  molecule, is analyzed in Fig. 1. In Fig. 1 (top panel), PIP-DMQMC is found to agree with DMQMC, IP-DMQMC, and ft-FCI by visual inspection. This was true across the whole data set but only corresponds to an accuracy of  $\sim 0.2$  Ha because the scale is so large. In Fig. 1 (bottom panel), we take a closer look at the systematic energy differences by subtracting the ft-FCI energy. For the range of  $\beta$  values studied, PIP-DMQMC consistently achieves equivalent or improved accuracy compared to DMQMC and IP-DMQMC, and its systematic error lies within 1mHa. In particular, in common with IP-DMQMC, it is able to improve upon the ‘shouldering’ seen in this DMQMC line – an increase in stochastic error at intermediate  $\beta$  values – which comes from loss of information from the diagonal of the density in DMQMC (this is which was what prompted the development of IP-DMQMC)<sup>65</sup>. PIP-DMQMC generally performs comparably with IP-DMQMC with the error for both methods falling well within the stated 1mHa accuracy target, though there is a difference in performance at  $\beta$  values between 5 and 10.

Figure 2 compares IP-DMQMC and PIP-DMQMC by looking at all of the test set data. In each case, differences were found between the method and ft-FCI and we are paying particular attention to the mHa error threshold. Here, we do find that IP-DMQMC has a drift towards lower values at intermediate  $\beta$  regimes in most cases which recovers at large  $\beta$ . A prominent example of this visible in Fig. 2 is stretched  $\text{H}_8$ , with a maximum deviation at around  $\beta = 10$ . Similar to DMQMC, this appears to be related to how the simulation is initialized; if a particular state is unlikely to be chosen there can

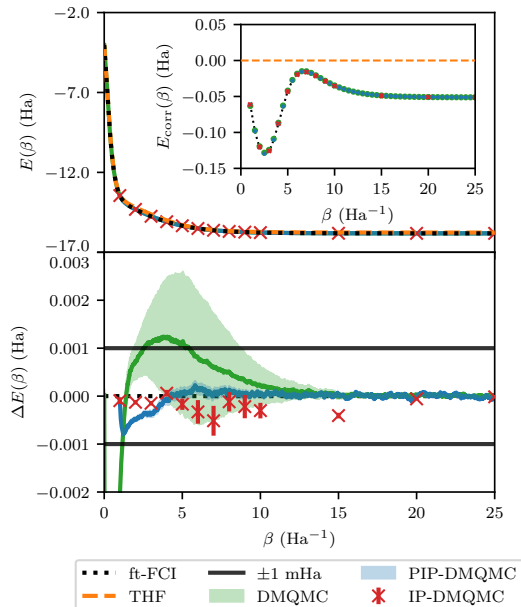


FIG. 1. Finite temperature energies for  $\text{BeH}_2$  Be/cc-pVDZ H/DZ from a variety of methods. In the top panel, total energies are shown plotted against  $\beta$ . Energies in the inset are calculated by taking the difference to THF, which is found with Eq. (15). The inset DMQMC and PIP-DMQMC data are re-sampled every 50 points starting from  $\beta = 1$ . In the bottom panel, energy differences with respect to ft-FCI are shown (when  $\Delta E$  is positive, ft-FCI is lower in energy). Data here show asymmetric PIP-DMQMC propagation (Eq. (21)). The PIP-DMQMC simulations were initialized with  $\beta_T = 1.0$ , allowing data collection at  $\beta \geq 1.0$ .

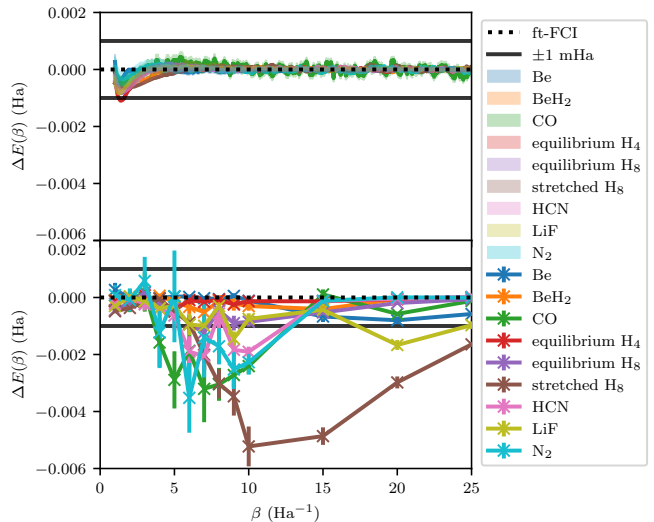


FIG. 2. Finite temperature energy differences to ft-FCI are shown for a variety of test systems for PIP-DMQMC (in the top panel) and IP-DMQMC (in the bottom panel). Data here show asymmetric PIP-DMQMC propagation (Eq. (21)). The PIP-DMQMC simulations were initialized with  $\beta_T = 1.0$ , allowing data collection at  $\beta \geq 1.0$ .

be errors due to under-sampling. This would ultimately be remedied if enough  $\beta$  loops were run. PIP-DMQMC appears to mostly remedy this, though we note that PIP-DMQMC does tend to have a dip in energy near its crossover point (where it switches propagator). Examples of this are  $\text{BeH}_2$  (Fig. 1), and CO in the supporting information.

Overall, therefore, we can conclude that PIP-DMQMC achieves just as good if not better energies than DMQMC and IP-DMQMC across our test set.

For all data presented so far, we have used a  $\beta_T = 1.0$  for PIP-DMQMC. Therefore it is worthwhile checking our conclusions for a range of  $\beta_T$  values to ensure they are not dependent on  $\beta_T$ . In Fig. 3(a) we plot PIP-DMQMC data for a range of  $\beta_T$  values from  $\beta_T = 1.0$  to  $\beta_T = 20.0$  using Eq. (21) for the  $\text{BeH}_2$  system.

The accuracy of PIP-DMQMC tended to remain similar or improve across the  $\beta_T$  used, supporting the prior conclusions made about the method. For the energy difference at  $\beta = \beta_T$ , the accuracy tended to be similar across all the  $\beta_T$  simulated. For the energy difference at  $\beta > \beta_T$ , the accuracy in general remained similar or shows slight improvement. The one exception being for  $\beta_T = 1.0$  where a notable decrease in accuracy is initially observed. Crucially all lines stay within the target accuracy of  $\pm 1$  mHa, which is too large to be shown on the plot range used in Fig. 3(a).

In addition to investigating the accuracy of PIP-DMQMC using several  $\beta_T$ , we investigate the variance of PIP-DMQMC in Fig. 3(b). Both PIP-DMQMC and IP-DMQMC methods have the same variance at  $\beta = \beta_T$  because we are using the same random number seed. In general the variance from PIP-DMQMC (run beyond the target  $\beta$ ) to the variance from IP-DMQMC, we see, in general, that the PIP-DMQMC variance is similar to or smaller than IP-DMQMC. This is to say that PIP-DMQMC's use of the Bloch equation tends to decrease variance relative to IP-DMQMC at  $\beta > \beta_T$ . One reason for this could be the way in which IP-DMQMC is initialized. We first recall that the Fermi-Dirac weights are used to select the diagonal matrix elements and that then these are re-weighted for the difference between the Fermi-Dirac density matrix and the Hartree-Fock density matrix (Eq. (17)). The re-weighting happens through spawning a certain number of walkers on this element. When the Fermi-Dirac density matrix is a poor match for the Hartree-Fock density matrix, the re-weighting will be large. However this, in turn, limits the high-energy rows that can be included in the simulation. Over successive  $\beta$  loops, our data are consistent with the idea that the variance due to this initialization is larger than propagating from an earlier  $\beta$  using the Bloch equation. The consequence of this is that more  $\beta$  loops may be required to convergence the stochastic error in IP-DMQMC as compared with PIP-DMQMC.

Our next test is to find out whether the initiator approximation works well with PIP-DMQMC. The initiator

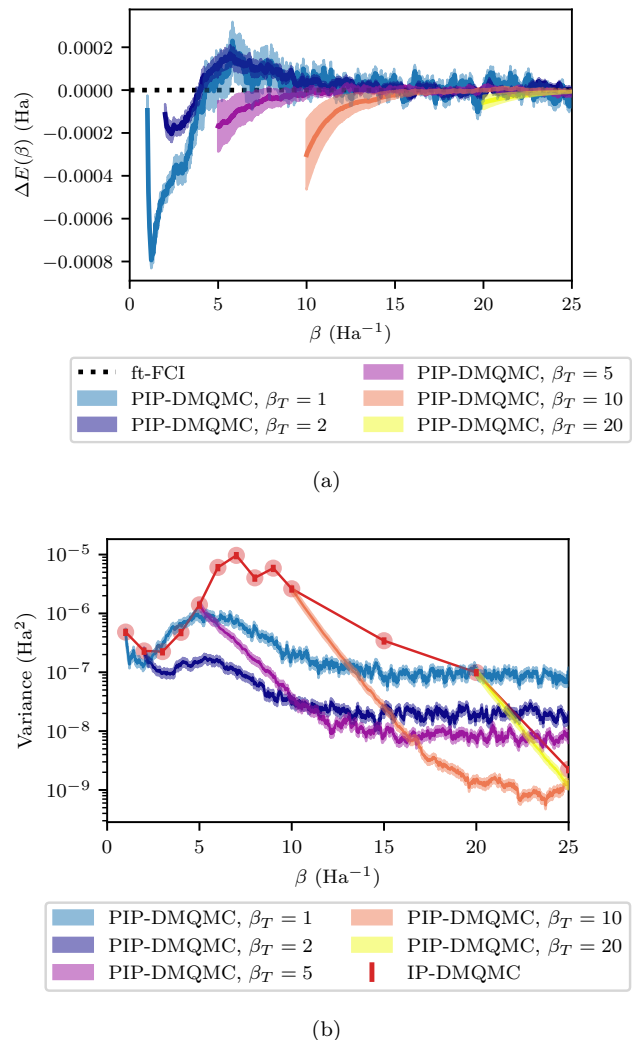


FIG. 3. Energy accuracy and variance of the PIP-DMQMC method using several  $\beta_T$  values (given in the legends) for  $\text{BeH}_2$   $\text{Be/cc-pVDZ H/DZ}$ . The impact of changing  $\beta_T$  for PIP-DMQMC is evaluated using: (a) the energy difference to the ft-FCI energy, and (b) the variance of the energy estimate compared to the IP-DMQMC variance. The  $\beta_T$  used for IP-DMQMC are the same as the  $\beta$  shown in the figure. PIP-DMQMC and IP-DMQMC have the same variance when the two share  $\beta_T$ . For  $\beta > \beta_T$ , the PIP-DMQMC variance is generally below that of IP-DMQMC. The PIP-DMQMC data shown are from asymmetric propagation (Eq. (21)). All data were collected using approximately ten million walkers ( $N_w = 10^7$ ) and averaged over 100  $\beta$  loops ( $N_\beta = 100$ ).

approximation is important for treating larger systems because the critical walker population (also known as a plateau height) rapidly grows beyond what we can store. We found that adding to the initiator space when the site has a population of 3 or greater ( $n_{\text{add}} = 3$ ) and having states be initiators if the bra and ket only differ by a double excitation ( $n_{\text{ex}} = 2$ ) gives reasonable results; these values were consistent with previous calculations in the uniform electron gas.<sup>74</sup> As  $n_{\text{ex}}$  causes the simulation to have a plateau again, we also must make sure we

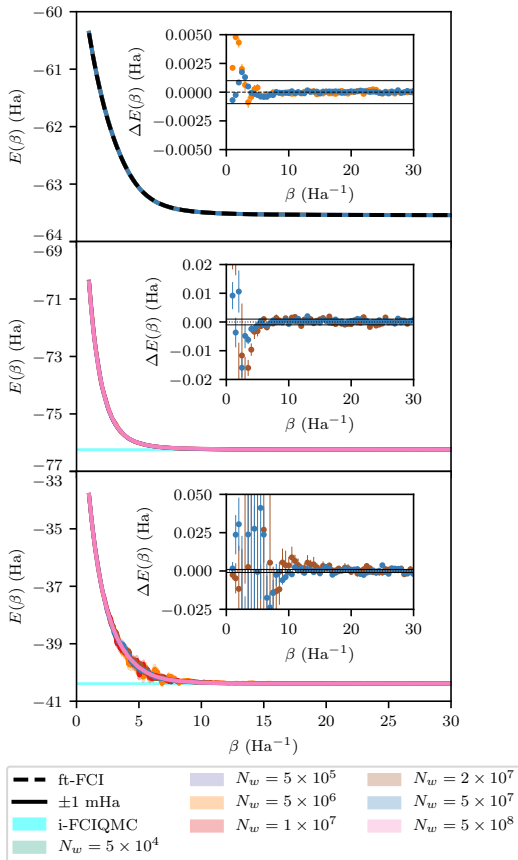


FIG. 4. Graphs to show initiator convergence for symmetric i-PIP-DMQMC (Eq. (20)) with increasing walker populations for HBCH<sub>2</sub>/STO-3G (top panel), H<sub>2</sub>O/cc-pVDZ (middle panel) and CH<sub>4</sub>/cc-pVDZ (bottom panel). Not all walker populations were run for all systems. Except for methane, the walker numbers fully overlap on the main graph. To show initiator convergence, the inset shows the energy calculated as a difference to the simulation with the largest walker population for CH<sub>4</sub> and H<sub>2</sub>O, and ft-FCI for HBCH<sub>2</sub>. The inset only shows the two largest walker populations to make trends more visible. Inset data are re-sampled every 50 points starting from  $\beta = 1$ . The largest walker population was  $5 \times 10^8$  for H<sub>2</sub>O and CH<sub>4</sub>.  $N_\beta$  was adjusted between population to give comparable error bars, the details of which are found in the supplementary information. The  $N_w = 5 \times 10^7$  for HBCH<sub>2</sub> and  $N_w = 5 \times 10^8$  for H<sub>2</sub>O contains one less  $\beta$ -loop compared to the other systems matching  $N_w$  data sets. The PIP-DMQMC simulations were initialized with  $\beta_T = 1.0$ , allowing data collection at  $\beta \geq 1.0$ .

are above the plateau to overcome the sign problem.

In Fig. 4, we show the results of the initiator adaptation with PIP-DMQMC (i-PIP-DMQMC) on three systems: HBCH<sub>2</sub>, H<sub>2</sub>O, and CH<sub>4</sub>. These calculations were run with a variety of walker numbers so that we could check for initiator convergence, which occurs when the walker number is increased without the energy changing.<sup>66,77,90</sup> In preliminary calculations, we noted relatively little difference between the two different modes of propagation and decided to use symmetric propagation (Eq. (20)) as this had been shown to reduce

stochastic noise in previous studies.<sup>81</sup>

In general, we see that the plots for different systems at different walker numbers generally overlay one another. The exception to this is low walker populations for CH<sub>4</sub>, and this is an example where the population is below the effective  $n_{\text{ex}} = 2$  plateau height at intermediate  $\beta$ . Each plot includes an inset where the difference is taken to the largest walker population for H<sub>2</sub>O and CH<sub>4</sub> and to ft-FCI for HBCH<sub>2</sub>. For HBCH<sub>2</sub>, we show the convergence to ft-FCI in the inset. At the highest walker population, the systematic error generally falls to  $\sim 1$ mHa for most  $\beta$  values. At its peak, the systematic error reaches  $\sim 2$ mHa at  $\beta$  at the highest population. For H<sub>2</sub>O and CH<sub>4</sub>, where we do not have ft-FCI results available, the inset instead shows the energy difference to the largest walker number (which is taken to be the best estimate we have). We find that, for high  $\beta$ , the initiator error is well converged. Between  $N_w = 5 \times 10^7$  and  $N_w = 5 \times 10^8$ , the energy difference is submillihartree above  $\beta > 5$  and  $\beta > 10$  for H<sub>2</sub>O and CH<sub>4</sub> respectively. For the smaller  $\beta$  values for both systems, the stochastic error rises sharply to an order of magnitude higher (i.e.  $\sim 0.01$ Ha). Any systematic initiator error is difficult to estimate due to this increase in stochastic error. In general, this shows significant promise for PIP-DMQMC and highlights the advantage of having so much data over the  $\beta$  range available.

One final consideration is that of computational cost. The cost ( $C$ ) of a simulation can be considered to be proportionate to the total amount of  $\beta$  that is simulated. In IP-DMQMC, sampling from an initial inverse temperature 0 to a final inverse temperature  $\beta$  with even spacing ( $\Delta\beta$ ) results in a cost:  $C \propto \beta \left( \frac{\beta}{2\Delta\beta} + \frac{1}{2} \right)$ . By contrast, PIP-DMQMC has a scaling of:  $C \propto \beta$ , which is the same as IP-DMQMC when  $\Delta\beta = 1$  and a temperature range is not being sampled. IP-DMQMC increases in cost as more  $\beta$  values are sampled and has an asymptotic scaling of  $\mathcal{O}(\beta^2)$ , while PIP-DMQMC costs  $\mathcal{O}(\beta)$ . In this way, PIP-DMQMC can be seen to both have an improved cost and resolution of the energy as a function of  $\beta$ .

## VI. CONCLUSIONS

In summary, we have introduced a piecewise generalization of the interaction picture propagator in density matrix quantum Monte Carlo, which leads to us being able to sample a wide range of temperatures with a single calculation. In proof of concept calculations on a variety of molecular systems, PIP-DMQMC is generally at least as accurate as IP-DMQMC and DMQMC. The result is a reduction in calculation cost to sample energies at 0 to  $\beta$  from  $\mathcal{O}(\beta^2)$  to  $\mathcal{O}(\beta)$  while also obtaining more data points. Furthermore, we see an improvement of sampling statistics especially at large  $\beta$  and have the ability to see more convergence data for the initiator approximation. We hope that others can use the water and methane cal-

culations for benchmarking their calculations.

Taken together, our results show that PIP-DMQMC is a promising development for DMQMC. Our long-term goal is to make DMQMC a resource for benchmarking finite temperature methods development<sup>8–21</sup> as well as describing electronic structure phenomena at finite temperature. With this in mind, two limitations of our study were that we did not systematically study convergence with initiator parameters or with starting initialization. These are interrelated because they both cause systematic biases in the energy and so efforts have to be made to separate out and measure the two effects. We are in the process of preparing a forthcoming manuscript on this topic.<sup>91</sup>

## VII. ACKNOWLEDGEMENTS

Research was supported by the U.S. Department of Energy, Office of Science, Office of Basic Energy Sciences Early Career Research Program (ECRP) under Award Number DE-SC0021317.

This research also used resources from the University of Iowa and the resources of the National Energy Research Scientific Computing Center, a DOE Office of Science User Facility supported by the Office of Science of the U.S. Department of Energy under Contract No. DE-AC02-05CH11231 (computer time for calculations only).

This research used a locally modified version of the development branch of HANDE-QMC.<sup>82</sup> The code will be queued for public release after the manuscript is published. For the purposes of providing information about the calculations used, files will be deposited with Iowa Research Online (IRO) with a reference number [to be inserted at production].

## VIII. DATA AVAILABILITY

The data that supports the findings of this study are available within the article.

- <sup>1</sup>B. Militzer, F. Soubiran, S. M. Wahl, and W. Hubbard, *Journal of Geophysical Research: Planets* **121**, 1552 (2016).
- <sup>2</sup>G. Mazzola, R. Helled, and S. Sorella, *Physical Review Letters* **120**, 025701 (2018).
- <sup>3</sup>S. Mukherjee, F. Libisch, N. Large, O. Neumann, L. V. Brown, J. Cheng, J. B. Lassiter, E. A. Carter, P. Nordlander, and N. J. Halas, *Nano Letters* **13**, 240 (2013).
- <sup>4</sup>L. Zhou, C. Zhang, M. J. McClain, A. Manjavacas, C. M. Krauter, S. Tian, F. Berg, H. O. Everitt, E. A. Carter, P. Nordlander, and N. J. Halas, *Nano Letters* **16**, 1478 (2016).
- <sup>5</sup>R. Ernstorfer, M. Harb, C. T. Hebeisen, G. Sciaini, T. Dartigalongue, and R. J. D. Miller, *Science* **323**, 1033 (2009).
- <sup>6</sup>E. Gull, O. Parcollet, and A. J. Millis, *Physical Review Letters* **110**, 216405 (2013).
- <sup>7</sup>N. D. Drummond, B. Monserrat, J. H. Lloyd-Williams, P. L. Ríos, C. J. Pickard, and R. J. Needs, *Nature Communications* **6**, 7794 (2015).
- <sup>8</sup>X. He, S. Ryu, and S. Hirata, *The Journal of Chemical Physics* **140**, 024702 (2014).
- <sup>9</sup>R. Santra and J. Schirmer, *Chemical Physics* **482**, 355 (2017).

- <sup>10</sup>S. Hirata and P. K. Jha, *The Journal of Chemical Physics* **153**, 014103 (2020).
- <sup>11</sup>P. K. Jha and S. Hirata, *Physical Review E* **101**, 022106 (2020).
- <sup>12</sup>S. Hirata, *The Journal of Chemical Physics* **155**, 094106 (2021).
- <sup>13</sup>A. A. Dzhioev and D. S. Kosov, *Journal of Physics A: Mathematical and Theoretical* **48**, 015004 (2015).
- <sup>14</sup>M. R. Hermes and S. Hirata, *The Journal of Chemical Physics* **143**, 102818 (2015).
- <sup>15</sup>F. Hummel, *Journal of Chemical Theory and Computation* **14**, 6505 (2018).
- <sup>16</sup>G. Harsha, T. M. Henderson, and G. E. Scuseria, *The Journal of Chemical Physics* **150**, 154109 (2019).
- <sup>17</sup>A. F. White and G. K.-L. Chan, *Journal of Chemical Theory and Computation* **15**, 6137 (2019).
- <sup>18</sup>P. Shushkov and T. F. Miller, *The Journal of Chemical Physics* **151**, 134107 (2019).
- <sup>19</sup>A. F. White and G. Kin-Lic Chan, *The Journal of Chemical Physics* **152**, 224104 (2020).
- <sup>20</sup>R. Peng, A. F. White, H. Zhai, and G. Kin-Lic Chan, *The Journal of Chemical Physics* **155**, 044103 (2021).
- <sup>21</sup>G. Harsha, Y. Xu, T. M. Henderson, and G. E. Scuseria, *Physical Review B* **105**, 045125 (2022).
- <sup>22</sup>V. V. Karasiev, T. Sjostrom, and S. B. Trickey, *Physical Review B* **86**, 115101 (2012).
- <sup>23</sup>J. A. Ellis, L. Fiedler, G. A. Popoola, N. A. Modine, J. A. Stephens, A. P. Thompson, A. Cangi, and S. Rajamanickam, *Physical Review B* **104**, 035120 (2021).
- <sup>24</sup>S. Pittalis, C. R. Proetto, A. Floris, A. Sanna, C. Bersier, K. Burke, and E. K. U. Gross, *Physical Review Letters* **107**, 163001 (2011).
- <sup>25</sup>H. Eschrig, *Physical Review B* **82**, 205120 (2010).
- <sup>26</sup>A. Pribram-Jones, P. E. Grabowski, and K. Burke, *Physical Review Letters* **116**, 233001 (2016).
- <sup>27</sup>A. A. Kananenka, A. R. Welden, T. N. Lan, E. Gull, and D. Zgid, *Journal of Chemical Theory and Computation* **12**, 2250 (2016).
- <sup>28</sup>A. R. Welden, A. A. Rusakov, and D. Zgid, *The Journal of Chemical Physics* **145**, 204106 (2016).
- <sup>29</sup>J. Kas and J. Rehr, *Physical Review Letters* **119**, 176403 (2017).
- <sup>30</sup>C. Karrasch, V. Meden, and K. Schönhammer, *Physical Review B* **82**, 125114 (2010).
- <sup>31</sup>D. Neuhauser, R. Baer, and D. Zgid, *Journal of Chemical Theory and Computation* **13**, 5396 (2017).
- <sup>32</sup>J. Gu, J. Chen, Y. Wang, and X.-G. Zhang, *Computer Physics Communications* **253**, 107178 (2020).
- <sup>33</sup>J. Li, M. Wallerberger, N. Chikano, C.-N. Yeh, E. Gull, and H. Shinaoka, *Physical Review B* **101**, 035144 (2020).
- <sup>34</sup>G. Knizia and G. K.-L. Chan, *Journal of Chemical Theory and Computation* **9**, 1428 (2013).
- <sup>35</sup>C. Sun, U. Ray, Z.-H. Cui, M. Stoudenmire, M. Ferrero, and G. K.-L. Chan, *Physical Review B* **101**, 075131 (2020).
- <sup>36</sup>J. S. Kretschmer and G. K.-L. Chan, *The Journal of Chemical Physics* **148**, 054108 (2018).
- <sup>37</sup>H. K. Tran, T. Van Voorhis, and A. J. W. Thom, *The Journal of Chemical Physics* **151**, 034112 (2019).
- <sup>38</sup>Z.-H. Cui, T. Zhu, and G. K.-L. Chan, *Journal of Chemical Theory and Computation* **16**, 119 (2020).
- <sup>39</sup>H. Zhai and G. K.-L. Chan, *The Journal of Chemical Physics* **154**, 224116 (2021).
- <sup>40</sup>T. Tsuchimochi, M. Welborn, and T. Van Voorhis, *The Journal of Chemical Physics* **143**, 024107 (2015).
- <sup>41</sup>I. W. Bulik, W. Chen, and G. E. Scuseria, *The Journal of Chemical Physics* **141**, 054113 (2014).
- <sup>42</sup>M. R. Hermes and L. Gagliardi, *Journal of Chemical Theory and Computation* **15**, 972 (2019).
- <sup>43</sup>D. Zgid and E. Gull, *New Journal of Physics* **19**, 023047 (2017).
- <sup>44</sup>T. N. Lan and D. Zgid, *The Journal of Physical Chemistry Letters* **8**, 2200 (2017).
- <sup>45</sup>L. N. Tran, S. Iskakov, and D. Zgid, *The Journal of Physical Chemistry Letters* **9**, 4444 (2018).



- <sup>46</sup>A. A. Rusakov, S. Iskakov, L. N. Tran, and D. Zgid, *Journal of Chemical Theory and Computation* **15**, 229 (2019).
- <sup>47</sup>T. Dornheim, S. Groth, A. Filinov, and M. Bonitz, *New Journal of Physics* **17**, 073017 (2015).
- <sup>48</sup>B. Militzer and K. P. Driver, *Physical Review Letters* **115**, 176403 (2015).
- <sup>49</sup>A. S. Larkin and V. S. Filinov, *Journal of Applied Mathematics and Physics* **05**, 392 (2017).
- <sup>50</sup>S. Groth, T. Dornheim, and M. Bonitz, *The Journal of Chemical Physics* **147**, 164108 (2017).
- <sup>51</sup>T. Dornheim, S. Groth, J. Vorberger, and M. Bonitz, *Physical Review Letters* **121**, 255001 (2018).
- <sup>52</sup>T. Dornheim, *Physical Review E* **100**, 023307 (2019).
- <sup>53</sup>A. Yilmaz, K. Hunger, T. Dornheim, S. Groth, and M. Bonitz, *The Journal of Chemical Physics* **153**, 124114 (2020).
- <sup>54</sup>T. Dornheim, M. Böhme, B. Militzer, and J. Vorberger, *Physical Review B* **103**, 205142 (2021).
- <sup>55</sup>C.-R. Lee, Z.-H. Chen, and Q.-L. Kao, in *2012 IEEE 26th International Parallel and Distributed Processing Symposium Workshops & PhD Forum* (IEEE, Shanghai, China, 2012) pp. 1889–1897.
- <sup>56</sup>C.-C. Chang, S. Gogolenko, J. Perez, Z. Bai, and R. T. Scalettar, *Philosophical Magazine* **95**, 1260 (2015).
- <sup>57</sup>Y. Liu, M. Cho, and B. Rubenstein, *Journal of Chemical Theory and Computation* **14**, 4722 (2018).
- <sup>58</sup>Y.-Y. He, M. Qin, H. Shi, Z.-Y. Lu, and S. Zhang, *Physical Review B* **99**, 045108 (2019).
- <sup>59</sup>T. Shen, Y. Liu, Y. Yu, and B. M. Rubenstein, *The Journal of Chemical Physics* **153**, 204108 (2020).
- <sup>60</sup>M. S. Church and B. M. Rubenstein, *The Journal of Chemical Physics* **154**, 184103 (2021).
- <sup>61</sup>Y. Liu, T. Shen, H. Zhang, and B. Rubenstein, *Journal of Chemical Theory and Computation* **16**, 4298 (2020).
- <sup>62</sup>N. Blunt, A. Alavi, and G. H. Booth, *Physical Review Letters* **115**, 050603 (2015).
- <sup>63</sup>N. S. Blunt, T. W. Rogers, J. S. Spencer, and W. M. C. Foulkes, *Physical Review B* **89**, 245124 (2014).
- <sup>64</sup>G. H. Booth, A. J. W. Thom, and A. Alavi, *The Journal of Chemical Physics* **131**, 054106 (2009).
- <sup>65</sup>F. D. Malone, N. S. Blunt, J. J. Shepherd, D. K. K. Lee, J. S. Spencer, and W. M. C. Foulkes, *The Journal of Chemical Physics* **143**, 044116 (2015).
- <sup>66</sup>D. Cleland, G. H. Booth, and A. Alavi, *The Journal of Chemical Physics* **132**, 041103 (2010).
- <sup>67</sup>T. Dornheim, S. Groth, F. D. Malone, T. Schoof, T. Sjoström, W. M. C. Foulkes, and M. Bonitz, *Physics of Plasmas* **24**, 056303 (2017).
- <sup>68</sup>S. Groth, T. Dornheim, T. Sjoström, F. D. Malone, W. Foulkes, and M. Bonitz, *Physical Review Letters* **119**, 135001 (2017).
- <sup>69</sup>T. Dornheim, S. Groth, T. Sjoström, F. D. Malone, W. Foulkes, and M. Bonitz, *Physical Review Letters* **117**, 156403 (2016).
- <sup>70</sup>H. R. Petras, S. K. Ramadugu, F. D. Malone, and J. J. Shepherd, *Journal of Chemical Theory and Computation* **16**, 1029 (2020).
- <sup>71</sup>H. R. Petras, W. Z. Van Benschoten, S. K. Ramadugu, and J. J. Shepherd, *Journal of Chemical Theory and Computation* **17**, 6036 (2021).
- <sup>72</sup>R. Chessex, M. Borrelli, and H. C. Öttinger, (2022), 10.48550/ARXIV.2201.01383, publisher: arXiv Version Number: 1.
- <sup>73</sup>Z. Kou and S. Hirata, *Theoretical Chemistry Accounts* **133**, 1487 (2014).
- <sup>74</sup>F. D. Malone, N. Blunt, E. W. Brown, D. Lee, J. Spencer, W. Foulkes, and J. J. Shepherd, *Physical Review Letters* **117**, 115701 (2016).
- <sup>75</sup>D. M. Cleland, G. H. Booth, and A. Alavi, *The Journal of Chemical Physics* **134**, 024112 (2011).
- <sup>76</sup>D. Cleland, G. H. Booth, C. Overy, and A. Alavi, *Journal of Chemical Theory and Computation* **8**, 4138 (2012).
- <sup>77</sup>J. J. Shepherd, G. H. Booth, and A. Alavi, *The Journal of Chemical Physics* **136**, 244101 (2012).
- <sup>78</sup>G. H. Booth, A. Grüneis, G. Kresse, and A. Alavi, *Nature* **493**, 365 (2013).
- <sup>79</sup>R. E. Thomas, G. H. Booth, and A. Alavi, *Physical Review Letters* **114**, 033001 (2015).
- <sup>80</sup>In the grand canonical initialization scheme introduced at the same time as IP-DMQMC<sup>65</sup>, the walker number was interpreted as the number of times initialization was attempted. For this paper, this was modified to instead count the number of walkers created.
- <sup>81</sup>F. D. Malone, *Quantum Monte Carlo Simulations of Warm Dense Matter*, Ph.D. thesis (2017).
- <sup>82</sup>J. S. Spencer, N. S. Blunt, S. Choi, J. Etrych, M.-A. Filip, W. M. C. Foulkes, R. S. T. Franklin, W. J. Handley, F. D. Malone, V. A. Neufeld, R. Di Remigio, T. W. Rogers, C. J. C. Scott, J. J. Shepherd, W. A. Vigor, J. Weston, R. Xu, and A. J. W. Thom, *Journal of Chemical Theory and Computation* **15**, 1728 (2019).
- <sup>83</sup>P. F. Bernath, A. Shayesteh, K. Tereszchuk, and R. Colin, *Science* **297**, 1323 (2002).
- <sup>84</sup>G. Herzberg, *Electronic spectra and electronic structure of polyatomic molecules*, Vol. 3 (van Nostrand, 1966).
- <sup>85</sup>M. Frisch, G. Trucks, H. B. Schlegel, G. E. Scuseria, M. A. Robb, J. R. Cheeseman, G. Scalmani, V. Barone, B. Mennucci, G. Petersson, and others, Inc., Wallingford CT **201** (2009).
- <sup>86</sup>F. Lovas, “Diatom Spectral Database, NIST Standard Reference Database 114,” (2002), type: dataset.
- <sup>87</sup>L. Wharton, W. Klemperer, L. P. Gold, R. Strauch, J. J. Gallagher, and V. E. Derr, *The Journal of Chemical Physics* **38**, 1203 (1963).
- <sup>88</sup>R. D. Johnson and others, <http://srdata.nist.gov/cccbdb> (2006).
- <sup>89</sup>H.-J. Werner, P. J. Knowles, G. Knizia, F. R. Manby, M. Schütz, and others, “MOLPRO, 2019.2, a package of ab initio programs,” (2019), see <https://www.molpro.net>.
- <sup>90</sup>G. H. Booth, D. Cleland, A. J. W. Thom, and A. Alavi, *The Journal of Chemical Physics* **135**, 084104 (2011).
- <sup>91</sup>W. Z. Van Benschoten and J. J. Shepherd, Unpublished.